

Spin transitions in the $\text{Fe}_x\text{Mn}_{1-x}\text{S}_2$ system

Kristin Persson and Gerbrand Ceder

Department of Materials Science and Engineering, Massachusetts Institute of Technology, Cambridge, Massachusetts 02139, USA

Dane Morgan

Department of Materials Science and Engineering, University of Wisconsin-Madison, Madison, Wisconsin 53706, USA

(Received 5 October 2005; revised manuscript received 11 January 2006; published 7 March 2006)

Pressure-induced spin transitions of the Fe^{2+} and the Mn^{2+} ions in the $\text{Fe}_x\text{Mn}_{1-x}\text{S}_2$ system are investigated using calculations based on density-functional theory within the generalized gradient approximation (GGA) + U formalism. MnS_2 shows a transition from a high-spin to a low-spin state at high pressure. The transition pressures decrease with increasing Fe content, and at high Fe content, transition pressures approaching zero are obtained. However, the volume change at the transition remains remarkably constant as long as both Fe and Mn participate.

DOI: [10.1103/PhysRevB.73.115201](https://doi.org/10.1103/PhysRevB.73.115201)

PACS number(s): 75.30.Kz, 64.70.-p, 71.30.+h, 71.20.-b

I. INTRODUCTION

Some $3d^n$ transition metal compounds exhibit a transition in spin state between a low-spin (LS) and a high-spin (HS) state.¹⁻¹⁰ In these materials, there is a competition between the interatomic crystal field ($10Dq$), which favors LS states, and the intra-atomic Hund exchange energy, which is minimized in the HS state. External influences such as temperature and/or pressure can shift the balance between these two and cause a spin transition. For an octahedrally coordinated transition metal, electrostatic theory predicts that the crystal field splitting, which manifests itself in the separation of the t_{2g} and e_g states, depends on the transition metal-ligand bond length as $10Dq \propto d_{\text{TM-ligand}}^{-5}$.¹¹ Thus, if external pressure is applied, the crystal field energy increases as the transition metal-ligand distances decrease. In addition, pressure drives electron delocalization, reducing the Hund coupling strength. High pressure also favors the LS state because the LS ion is generally smaller than the HS ion. This size difference results in a smaller pV contribution to the enthalpy for the LS state, thus lowering the enthalpy compared to the HS state. Under increasing pressure the cumulative effect of increasing crystal field energy and the pV term overcomes the weakening Hund coupling, causing a transition from a HS to a LS state. These transitions can exhibit both first and second order transition characteristics. For example, the temperature-induced LS to HS transitions⁴⁻⁶ in LaCoO_3 show a smooth volume and bond-length dependence on temperature. On the other hand, FeBO_3 , LaFeO_3 , and NdFeO_3 provide three examples of materials with discontinuous pressure-induced spin transitions with volume changes between 3 and 9%.⁷⁻⁹

Spin transitions are interesting to study from a theoretical electronic structure point of view. Although extensively observed and studied in molecular crystals and polymers,^{11,12} so far, spin transitions in bulk materials are relatively rare. From a technological point of view, spin crossover molecular materials have already attracted interest for applications in areas such as memory devices, sensors, and displays.¹² The dramatic lattice parameter changes, which result from a pressure-induced spin transition in a bulk material, could po-

tentially be of technological use. In this work we demonstrate an approach to increase the possible applications of a material with an existing spin transition by tuning the transition pressure as a function of composition.

As an example of this compositional tuning we have chosen a combination of compounds for which the magnetovolume effect is predicted to be especially large. Magnetic moments in the pyrite-structured semiconductor MnS_2 order antiferromagnetically along a wave vector of $(\mathbf{k}=\mathbf{1}, \frac{1}{2}, \mathbf{0})$ (Ref. 13) below $T_N=48.2$ K.¹⁴⁻¹⁶ At T_N the crystal undergoes a first-order magnetic transition, upon heating, to the paramagnetic phase via a frustrated antiferromagnet with an incommensurate wave vector $\mathbf{k}=(1, k_y, 0)$.^{17,18} At ambient conditions, in an octahedral environment, the Mn^{2+} ion has the d^5 ($3t_{2g}\uparrow 2e_g\uparrow, S=5/2$) electronic configuration. This HS arrangement of the Mn^{2+} ion yields a large unit cell volume for a pyrite-structured transition metal disulphide. As pressure is applied, one expects the electronic configuration of the manganese ion to change to $3t_{2g}\uparrow 2t_{2g}\downarrow$ ($S=1/2$), due to the increased crystal field splitting. There is experimental evidence of a pressure-induced first order structural transformation in MnS_2 from pyrite into marcasite around 12.3–16.8 GPa,^{19,20} accompanied by a 15% volume contraction. The marcasite structure is an orthorhombic distortion of the cubic pyrite structure. Coexistence of both structures over a wide range of pressure is observed. Chattopadhyay *et al.*^{19,20} suggest that this structural transformation is caused by an electronic HS-LS transition and possibly accompanied by an insulator-metal transition. Recently, a HS-LS transition in pyrite-structured MnS_2 was theoretically predicted to occur around 11–16 GPa,²¹ without considering the structural transformation. A similar spin transition has also been found experimentally in MnTe_2 at 8 GPa, together with an insulator-metal transition.^{22,23}

A lower spin transition pressure would make the transition more accessible for practical applications. We propose to tune the transition pressure by substituting Fe^{2+} for Mn^{2+} in the pyrite structure. FeS_2 is a low-spin semiconductor with a particularly low unit cell volume for a pyrite-structured transition metal disulphide. Dilute substitutions of 0.5–2% Fe^{2+}

into pyrite MnS_2 have been experimentally investigated using the Mössbauer technique.^{31,32} Kahn *et al.*³² show that, while Fe^{2+} is LS in FeS_2 , the Fe^{2+} ions in the MnS_2 lattice are exclusively in the HS configuration. The direction of the exchange field in Fe-doped MnS_2 is also measured,³² and the result implies the existence of a multiaxis spin system which suggests weak magnetic interaction between the Fe^{2+} and Mn^{2+} ions. The HS configuration of the Fe^{2+} ions in MnS_2 can therefore be rationalized by the fact that, due to the large size of the Mn^{2+} ion, the Fe-S distances in dilute $\text{Fe}_x\text{Mn}_{1-x}\text{S}_2$ are likely to be much larger than in FeS_2 , which thereby reduces the crystal field splitting. Furthermore, in Ref. 31 it is shown that the Fe^{2+} ions in Fe-doped MnS_2 undergo a HS to LS transition as a function of pressure between 4 and 12 GPa.

In Sec. II we present some details on the electronic structure calculations for the $\text{Fe}_x\text{Mn}_{1-x}\text{S}_2$ system. In Secs. III A and III B we compare the ground state properties calculated with the generalized gradient approximation (GGA) and GGA+ U method and discuss the results for the different transition metal sulphides. Furthermore, we calculate the spin transition pressures for intermediate compositions in the $\text{Fe}_x\text{Mn}_{1-x}\text{S}_2$ system and present the results in Sec. III C. We show that the spin transition pressures decrease with increasing Fe content. At high Fe content our results predict the lowest (to the best of our knowledge) spin transition pressure in a solid. In Sec. III D we present analyses of transition metal-ligand bond length developments and spin transition volume changes as a function of composition. Finally, our conclusions are given.

II. STRUCTURAL DETAILS AND COMPUTATIONAL METHODS

MnS_2 and FeS_2 crystallize in the pyrite structure whose symmetry belongs to the $Pa\bar{3}$ space group. The pyrite structure has 12 atoms/cell, containing four symmetry equivalent transition metal ions each, in a slightly distorted octahedral environment of sulphur ions. Antiferromagnetic ordering doubles the unit cell of MnS_2 along one of the cubic $\langle 100 \rangle$ directions, giving a 24 atom unit cell for MnS_2 .^{18,32} To study intermediate compositions in $\text{Fe}_x\text{Mn}_{1-x}\text{S}_2$, some of the Mn^{2+} ions are substituted by Fe^{2+} ions in the cell. Substitutions are always made in pairs, replacing majority and minority spin Mn simultaneously, and the Fe moments are given the same direction as the Mn atoms which they replace. This method of substitution effectively leaves the MnS_2 antiferromagnetic ordering unchanged for all compositions and keeps the overall magnetic moment of the system at zero. Substituting two metal ions at a time in the 8 metal atom cell allows alloy compositions of $x=0.25$, 0.50, and 0.75. Additionally, a 48 atom $[2 \times 1 \times 2]$ supercell, calculation of the $x=0.875$ composition is made. Subject to the magnetic constraints just described, two permutations with different local orderings on the transition metal lattice are calculated for each composition, see the Appendix. We restrict our calculations to the pyrite structure as the change in electronic state is likely the driving mechanism for the experimentally observed structural transformation and not the reverse. This approach also

makes it easier to focus on the analyses of the electronic changes without obscuring the picture with cell shape changes.

The electronic ground state of each compound is obtained using the GGA/GGA+ U method with the projector-augmented plane-wave (PAW) method^{33,34} as implemented in the Vienna Ab-initio Simulation Package (VASP).^{35,36} For sulphur we have chosen the standard $3s^23p^4$ pseudopotential, but to ensure accuracy when pressure is applied the transition metal pseudopotentials include $3p^6$ semicore states in addition to the $3d^n4s^2$ configuration. To sample the band structure, the Brillouin zone integration is performed using Monkhorst-Pack grids³⁷ varying from $1 \times 3 \times 3$ to $2 \times 4 \times 4$. Testing with denser grids (up to $8 \times 8 \times 8$) ensured that HS-LS total energy differences are converged to ≤ 2 meV/formula unit (f.u.) with respect to k -point sampling. For calculation of the total energy the tetrahedron method³⁸ with Blöchl corrections is used. The plane-wave cutoff is fixed to 300 eV. Testing with a higher cutoff energy of 400 eV showed that HS-LS energy differences are converged to within 4 meV/f.u. with respect to the basis set. We employ the GGA formulation as in Ref. 39. Additionally, for the transition metals we use the GGA+ U implementation of Liechtenstein *et al.*⁴⁰ where the Hubbard U and the exchange parameter J enter separately. The Mn d orbitals are consistently described with $U=3$ eV, which has recently been shown to yield good agreement²¹ with experimentally obtained ground state properties. In the case of FeS_2 we employ both $U=3$ eV, which we will argue improves the description of Fe^{2+} in the pyrite structure compared to GGA, and $U=0$ eV for comparison. When GGA+ U is applied ($U \neq 0$), we use $J=1$ eV, which has previously been successfully applied to MnS_2 and other Mott insulators.^{21,40} Preparation and analysis of VASP files was done primarily with the CONVASP code.⁴¹

III. RESULTS AND DISCUSSION

A. Calculated ground state properties for MnS_2 using GGA+ U

Experimentally, MnS_2 is found to be a HS Mott insulator with a gap of 1 eV.²⁹ The unit cell volume and bulk modulus of MnS_2 are, respectively, $56.28 \text{ \AA}^3/\text{f.u.}$ and 76 GPa,^{19,24} cf. Table I. GGA calculations⁴² predict MnS_2 to be a LS zero-gap semiconductor with an equilibrium volume of $42.6 \text{ \AA}^3/\text{f.u.}$ These discrepancies are remedied²¹ by improving the treatment of the electron correlation on the metal d -states through an onsite Hubbard U as in the GGA+ U method. It has been found that ground state properties such as the band gap and the equilibrium volume of MnS_2 are best described by a weak $U_{\text{Mn}}=3$ eV.²¹ Our calculations for MnS_2 yield results very similar to those presented in Ref. 21. In Table I we compare our calculated ground state properties of MnS_2 for $U_{\text{Mn}}=3$ and $J=1$ eV with experimental results. All calculated equations of state are fit with the Murnaghan form.⁴³ Overall, we obtain a very good agreement between experimental and calculated structural ground state properties.

TABLE I. Ground state properties for MnS_2 and FeS_2 calculated with the GGA and GGA+ U ($U_{\text{Mn}}=U_{\text{Fe}}=3$, $J=1$ eV) method and compared with experiments.

Properties	MnS_2		FeS_2		
	GGA+ U	Expt.	GGA	GGA+ U	Expt.
V_0 ($\text{\AA}^3/\text{f.u.}$)	57.39	56.28 ^a	39.51	39.69	39.717 ^b
B (GPa)	60	76 ^c	154	138	133.5 \pm 5.2 ^d
B'	3.1	5.4 ^c	4.5	4.8	5.73 \pm 0.58 ^c
m (μ_B/ion)	4.54	5 ^e	0	0	0
band gap (eV)	1.0	1.0 ^f	0.5	1	0.95 ^g
$d_{\text{S-S}}$ (\AA)	2.09	2.091 ^a	2.19	2.15	2.153 ^h , 2.1604 ^b
$d_{\text{TM-S}}$ (\AA)	2.58	2.591 ^a	2.25	2.26	2.259 ^h
$d_{\text{TM-TM}}$ (\AA)	4.29	4.30 ^a	3.51	3.83	3.83 ^b

^aReference 24.^bReference 25.^cReference 19.^dReference 26.^eReference 27.^fReference 28.^gReference 29.^hReference 30.

In Table II some spin transition related properties for MnS_2 are listed. At zero pressure, we find the LS state of MnS_2 to be 720 meV/f.u. higher in energy and 12.3 $\text{\AA}^3/\text{f.u.}$ smaller in unit cell volume than the ground state. At the transition pressure of 11.5 GPa, the induced volume change is 9.6 $\text{\AA}^3/\text{f.u.}$ For $3 \leq U_{\text{Mn}} \leq 4.5$ eV the spin transition pressure (without any structural transformation) is bracketed between 11 and 16 GPa,²¹ to be compared with the experimental structural transition pressure of 12–16.8 GPa.^{19,20}

Figure 1 shows the Mn d density of states (DOS) for the HS and LS state of pyrite MnS_2 . The distortion of the MnS_2 octahedra lowers the symmetry of the crystal field at the manganese site from cubic to trigonal and the t_{2g} are split into two sublevels. However, the deviations from cubic symmetry are small and the crystal field is still dominated by its cubic part. The occupied HS DOS shows the localized t_{2g} states and the delocalized bonding and antibonding e_g states, in agreement with previous calculations.²¹ In the LS state the t_{2g} orbitals have moved closer to the Fermi energy. Assuming that the Hubbard U for the Mn d orbitals does not change significantly from the HS to the LS state, we observe that pyrite MnS_2 remains semiconducting in its LS state with a band gap of 0.5 eV.

B. Calculated ground state properties for FeS_2 using GGA and GGA+ U

Experimentally, pyrite FeS_2 is found to be a LS semiconductor with a band gap of 0.95 eV.²⁹ X-ray diffraction ex-

TABLE II. Spin transition properties in FeS_2 and MnS_2 with $U_{\text{Mn}}=U_{\text{Fe}}=3$, $J=1$ eV. $\Delta E_p^{\text{HS-LS}}$ and $\Delta V_p^{\text{HS-LS}}$ are evaluated at the transition pressure.

Properties	MnS_2	FeS_2
$\Delta E_p^{\text{HS-LS}}$ (meV/f.u.)	-660	90
$\Delta V_p^{\text{HS-LS}}$ ($\text{\AA}^3/\text{f.u.}$)	9.6	11.7
$P_{\text{HS-LS}}$ (GPa)	11.5	-1.2

periments show an absence of structural phase transitions up to almost 50 GPa [Ref. 26 and references therein]. Several theoretical studies^{44–48} have shown that the broad features of pyrite FeS_2 are correctly predicted using the GGA/LDA (local density approximation). However, the band gap is underestimated by 0.1–0.6 eV,^{44,47} depending on the method used, and the bulk modulus is generally too high with values around 150–170 GPa.^{46,49} From Table I we observe that including a weak U on the d orbitals of Fe^{2+} ion improves the agreement between experiments and calculations with respect to band gap, bulk modulus, and interatomic distances, compared to the GGA.

Most importantly, we find that a HS state (antiferromagnetic or ferromagnetic) in FeS_2 cannot be obtained, even as a metastable state, in the GGA at zero pressure without explicitly constraining the magnetic moment. Only for negative pressures ($p \leq -9$ GPa) can a metastable antiferromagnetic state be obtained. However, applying a weak Hubbard U to the Fe d orbitals stabilizes a metastable HS antiferromagnetic FeS_2 state. Therefore, given the observation of an equilibrium HS Fe^{2+} state as a dilute dopant in the MnS_2 ,³¹ together with the excellent agreement between GGA+ U calculated and experimental ground state properties in FeS_2 , we suggest that GGA+ U provides an overall better description of the physical properties of the Fe^{2+} ion in the pyrite structure. In Table II we show the HS-LS equilibrium energy and volume differences at the spin crossover pressure of -1.2 GPa for iron disulphide with $U_{\text{Fe}}=3$ eV. The HS antiferromagnetic state in FeS_2 is metastable with an equilibrium energy 90 meV/f.u. higher than the LS ground state. We observe that the HS-LS energy difference is about $\frac{1}{8}$ times the value in MnS_2 which is also reflected in the small absolute value of the spin transition pressure in FeS_2 .

In Fig. 2 the HS and LS d DOS for FeS_2 are presented. LS FeS_2 exhibits a clear separation of t_{2g} and e_g states. The t_{2g} orbitals form localized states in the upper valence band whereas the e_g orbitals are divided into occupied bonding states around -3 eV and antibonding nonoccupied states around 2.5 eV. In HS FeS_2 the crystal field splitting is less pronounced. We find that the HS band gap has closed which

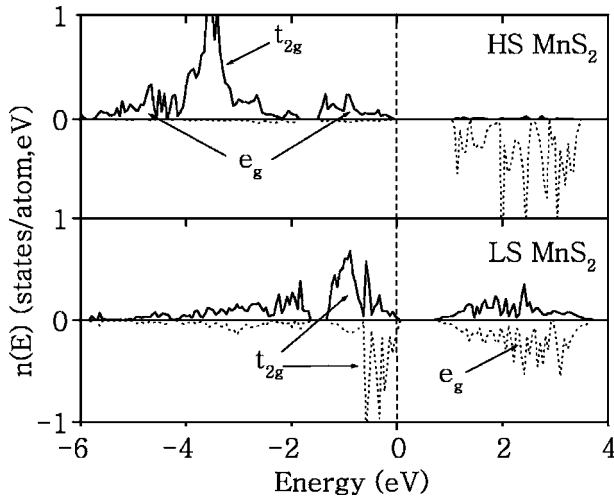


FIG. 1. HS and LS MnS_2 d density of states for $U_{\text{Mn}}=3$ eV at zero pressure. Majority spin (solid lines) and minority spin (dotted lines) are plotted separately. Arrows indicate regions which are primarily of t_{2g} or e_g character.

should make the conductivity of FeS_2 in HS configuration noticeably higher than in its LS state.

C. Energetics and spin transitions in $\text{Fe}_x\text{Mn}_{1-x}\text{S}_2$

To investigate spin transitions in the mixed $\text{Fe}_x\text{Mn}_{1-x}\text{S}_2$ system we explore two possible arrangements of the Mn^{2+} and Fe^{2+} ions at each composition possible in the 24 atom cell (see the Appendix). We find only small energy differences (≤ 30 meV/f.u.) for the different local orderings on the transition metal lattice. The ordered arrangement with the lowest $p=0$ equilibrium energy is used for all compositions. Also, we find that the specific configuration of Fe and Mn on the transition metal lattice does not significantly influence the relative stability between the LS and HS states. Thus, the spin transition pressure between the two ordered structures with the same composition differ by as little as 0.1 GPa.

When pressure is applied to the $\text{Fe}_x\text{Mn}_{1-x}\text{S}_2$ system the transition metal ions are driven to the LS state. We find that, as a function of increasing Fe content, the spin transition pressure decreases. However, depending on the actual composition and whether GGA or GGA+ U is used for the Fe d orbitals, the transition process is different. Within the GGA, the Fe^{2+} ion is in the LS state at all pressures. Thus, only the Mn^{2+} ion undergoes a spin transition under pressure and the only possible phase transition is between $\text{Mn}^{\text{HS}}\text{Fe}^{\text{LS}}$ and $\text{Mn}^{\text{LS}}\text{Fe}^{\text{LS}}$. When a Hubbard U is applied to the Fe d orbitals, two distinct scenarios are possible; either the spin transitions for both Fe and Mn occur collectively, i.e., $\text{Mn}^{\text{HS}}\text{Fe}^{\text{HS}}$ transforms directly into the $\text{Mn}^{\text{LS}}\text{Fe}^{\text{LS}}$ state or the spin transitions occur separately, i.e., $\text{Mn}^{\text{HS}}\text{Fe}^{\text{HS}}$ transforms to $\text{Mn}^{\text{HS}}\text{Fe}^{\text{LS}}$, a mixed spin state, and then to $\text{Mn}^{\text{LS}}\text{Fe}^{\text{LS}}$. The mixed spin state needs to accommodate both the small LS Fe^{2+} and the large HS Mn^{2+} . Hence a considerable strain energy is expected in this mixed state and one expects the $\text{Mn}^{\text{HS}}\text{Fe}^{\text{LS}}$ state to display large differences in local relaxations around the HS and LS ions. This size mismatch will also manifest itself in the

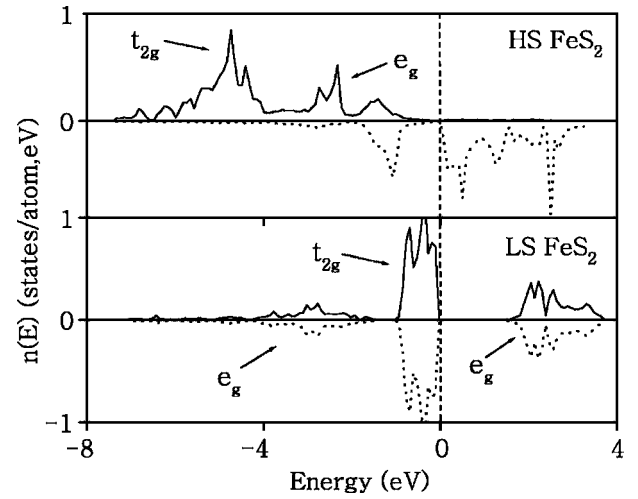


FIG. 2. HS and LS FeS_2 d density of states for $U_{\text{Fe}}=3$ eV at zero pressure. Majority spin (solid lines) and minority spin (dotted lines) are plotted separately. Arrows indicate regions which are primarily of t_{2g} or e_g character.

energetics of the alloy. The total elastic energy required to deform the HS Mn^{2+} and the LS Fe^{2+} to an intermediate volume is positive throughout the composition range and is expected to reach its maximum at $x=0.50$, similar to the elastic contribution to mixing enthalpy of A and B atoms with different size. We believe that, at $x=0.50$, the elastic penalty of the mixed spin state is too high and it does not appear as a function of pressure. Rather, a single transition from $\text{Mn}^{\text{HS}}\text{Fe}^{\text{HS}}$ to $\text{Mn}^{\text{LS}}\text{Fe}^{\text{LS}}$ occurs. At lower or higher Fe compositions, the strain energy of the mixed spin state is less and it can occur as an intermediate between the complete HS and LS states.

Figure 3 shows the energy as a function of volume for $x=0.25$ in $\text{Fe}_x\text{Mn}_{1-x}\text{S}_2$ with $U_{\text{Fe}}=0$ (GGA) and $U_{\text{Fe}}=3$ eV. At $x=0.25$, we find for $U_{\text{Fe}}=0$ that the Fe^{2+} HS state is only stable for $p < 0$ GPa (cf., Fig. 3). The stable state at $p=0$ is the $\text{Mn}^{\text{HS}}\text{Fe}^{\text{LS}}$ configuration. At $p=6.8$ GPa, we obtain the $\text{Mn}^{\text{HS}}\text{Fe}^{\text{LS}}-\text{Mn}^{\text{LS}}\text{Fe}^{\text{LS}}$ transition. The $U_{\text{Fe}}=3$ eV results agree better with experimental evidence. For lower pressures, the $\text{Mn}^{\text{HS}}\text{Fe}^{\text{HS}}$ state is stable. At $p=5$ GPa, the Fe ion goes through the HS-LS transition and the $\text{Mn}^{\text{HS}}\text{Fe}^{\text{LS}}$ state is obtained. Note that the $p=0$ equilibrium volume of the $\text{Mn}^{\text{HS}}\text{Fe}^{\text{LS}}$ state is close, $\Delta V_0(\text{Mn}^{\text{HS}}\text{Fe}^{\text{HS}}-\text{Mn}^{\text{HS}}\text{Fe}^{\text{LS}}) = 1.8 \text{ \AA}^3/\text{f.u.}$, to the equilibrium volume of the $\text{Mn}^{\text{HS}}\text{Fe}^{\text{HS}}$ state, which is reasonable as the cell is dominated by HS Mn^{2+} . Further increasing the pressure to 8.7 GPa yields the $\text{Mn}^{\text{LS}}\text{Fe}^{\text{LS}}$ state.

For the $x=0.50$ composition, when the Fe d orbitals are described within the GGA, we find that the $\text{Mn}^{\text{HS}}\text{Fe}^{\text{LS}}-\text{Mn}^{\text{LS}}\text{Fe}^{\text{LS}}$ transition occurs at 3.8 GPa (see Fig. 5). For $U_{\text{Fe}}=3$ eV, the mixed $\text{Mn}^{\text{HS}}\text{Fe}^{\text{LS}}$ state is bypassed, and the spin transitions occur collectively from the $\text{Mn}^{\text{HS}}\text{Fe}^{\text{HS}}$ to the $\text{Mn}^{\text{LS}}\text{Fe}^{\text{LS}}$ state, at 5 GPa. This can be rationalized by the large differences in ionic sizes between the HS Mn^{2+} and the LS Fe^{2+} ions, which will affect the energetics of the mixed spin state maximally at the $x=0.50$ composition. The equilibrium volume of the mixed spin state $\text{Mn}^{\text{HS}}\text{Fe}^{\text{LS}}$ is significantly smaller than that of the HS state at $x=0.50$ compared

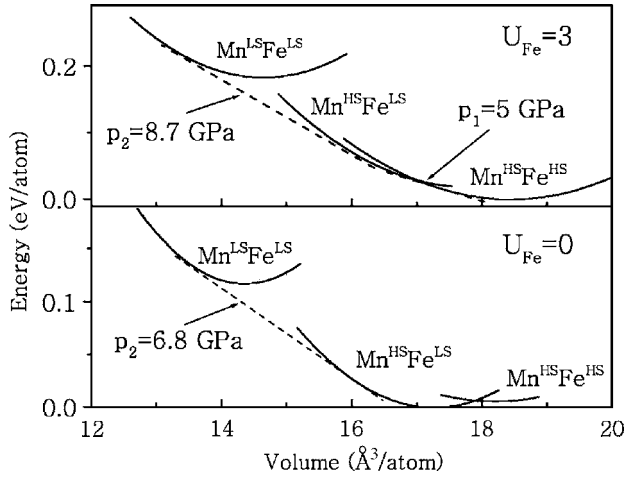


FIG. 3. Energy vs volume curves for $\text{Fe}_{0.25}\text{Mn}_{0.75}\text{S}_2$ for $U_{\text{Fe}}=0$ and $U_{\text{Fe}}=3$ eV.

to at $x=0.25$ [$\Delta V_0(\text{Mn}^{\text{HS}}\text{Fe}^{\text{HS}}-\text{Mn}^{\text{HS}}\text{Fe}^{\text{LS}})=6.9 \text{ \AA}^3/\text{f.u.}$ at $x=0.50$ vs $1.8 \text{ \AA}^3/\text{f.u.}$ at $x=0.25$]. This difference reflects the increased number of small LS Fe^{2+} ions in the cell and results in a large deformation energy for the HS Mn^{2+} ions. The equal spin transition pressures (i.e., the complete suppression of the mixed spin state) at $x=0.50$ could be an effect of the specific supercell employed. However, due to the size argument, we expect the spin transition pressures for the two transition metal ions in $\text{Fe}_x\text{Mn}_{1-x}\text{S}_2$ to be very close to each other at the 50% composition, regardless of the supercell.

Figure 4 shows the energy vs volume curves for the different spin states at the $x=0.75$ composition. For $U_{\text{Fe}}=0$, the $\text{Mn}^{\text{LS}}\text{Fe}^{\text{LS}}$ state is the equilibrium state at zero pressure. Thus, within the GGA, an absence of spin transition is predicted for this composition. Applying a $U_{\text{Fe}}=3$ eV to the Fe d orbitals, we obtain the $\text{Mn}^{\text{HS}}\text{Fe}^{\text{HS}}-\text{Mn}^{\text{HS}}\text{Fe}^{\text{LS}}$ transition at 0.6 GPa, followed by the $\text{Mn}^{\text{HS}}\text{Fe}^{\text{LS}}-\text{Mn}^{\text{LS}}\text{Fe}^{\text{LS}}$ transition at 3.3 GPa. We find that the $\text{Mn}^{\text{HS}}\text{Fe}^{\text{LS}}$ state is realized at intermediate pressures. The unit cell volume of the $\text{Mn}^{\text{HS}}\text{Fe}^{\text{LS}}$ state is small, compared to the equilibrium volume of HS MnS_2 , which is unfavorable for the HS Mn^{2+} ions. However, the unit cell is now dominated by LS Fe^{2+} which makes the overall state energetically stable. For the $x=0.875$ calculation and $U_{\text{Fe}}=3$ eV, the $\text{Mn}^{\text{LS}}\text{Fe}^{\text{LS}}$ state is the equilibrium state at zero pressure and thus, no spin transition is obtained (see Fig. 5).

Figure 5 and Table III summarize the transition pressures

TABLE III. Spin transition pressures for $\text{Mn}^{\text{HS}}\text{Fe}^{\text{HS}}-\text{Mn}^{\text{HS}}\text{Fe}^{\text{LS}}$ (p_1) and $\text{Mn}^{\text{HS}}\text{Fe}^{\text{LS}}-\text{Mn}^{\text{LS}}\text{Fe}^{\text{LS}}$ (p_2) as a function of composition x in $\text{Fe}_x\text{Mn}_{1-x}\text{S}_2$ with $U_{\text{Fe}}=0$ and $U_{\text{Fe}}=3$ eV.

x	$U_{\text{Fe}}=0$		$U_{\text{Fe}}=3$	
	p_2	p_1	p_1	p_2
0	11.5			11.5
0.25	6.9	5	8.7	
0.5	3.8	5	5	
0.75	0	0.6	3.3	

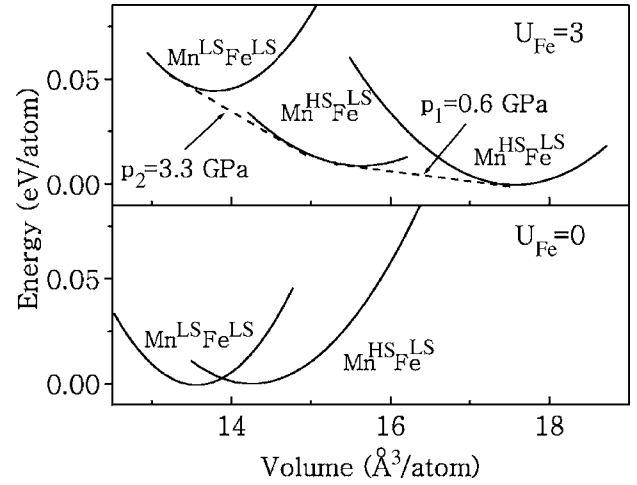


FIG. 4. Energy vs volume curves for $\text{Fe}_{0.75}\text{Mn}_{0.25}\text{S}_2$ for $U_{\text{Fe}}=0$ and $U_{\text{Fe}}=3$ eV.

for all compositions. In Fig. 5, the solid lines depict the spin transition pressures for the two transition metal species for $U_{\text{Fe}}=3$ eV. The dashed line represents the spin transition pressures for the Mn ion (as Fe is LS for all concentrations when $U_{\text{Fe}}=0$). We note that the choice of $0 \leq U_{\text{Fe}} \leq 3$ eV does not influence the general observation that in the $\text{Fe}_x\text{Mn}_{1-x}\text{S}_2$ system there exists a composition for which the spin transition pressure approaches zero. For $U_{\text{Fe}}=0$, this composition is slightly below $x=0.75$ and for $U_{\text{Fe}}=3$ eV it is slightly above $x=0.75$. The decreasing trend of the spin transition pressures with increasing Fe content is clear, independent of our choice of U_{Fe} .

D. Bond length and volume development

In the pyrite structure, every transition metal ion is surrounded by six nearest-neighbor (NN) sulphur ions. The sul-

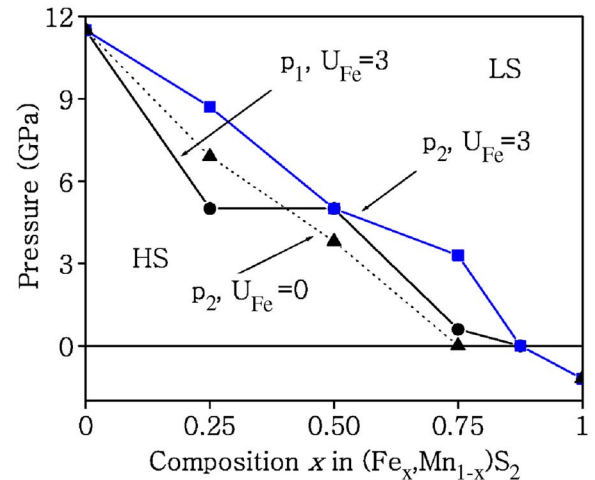


FIG. 5. (Color online) Spin transition pressures as a function of composition x in $\text{Fe}_x\text{Mn}_{1-x}\text{S}_2$ for $U_{\text{Fe}}=0$ (dashed line with triangles) and $U_{\text{Fe}}=3$ eV (solid lines). The spin transition from $\text{Mn}^{\text{HS}}\text{Fe}^{\text{HS}}$ to $\text{Mn}^{\text{HS}}\text{Fe}^{\text{LS}}$ is denoted by p_1 (circles) and the transition from $\text{Mn}^{\text{HS}}\text{Fe}^{\text{LS}}$ to $\text{Mn}^{\text{LS}}\text{Fe}^{\text{LS}}$ is represented by p_2 (squares).

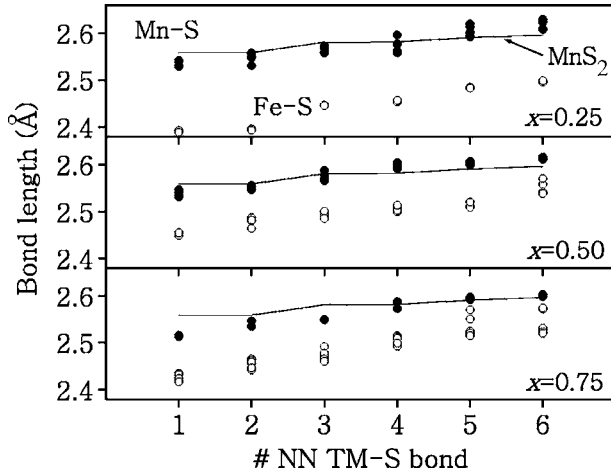


FIG. 6. Calculated nearest neighbor HS TM-S bond lengths at $p=0$ at $x=0.25, 0.50,$ and 0.75 for $U_{\text{Fe}}=3$ eV. Filled symbols (\bullet) denote Mn-S bonds in $\text{Fe}_x\text{Mn}_{1-x}\text{S}_2$, while open symbols (\circ) represent Fe-S bonds in $\text{Fe}_x\text{Mn}_{1-x}\text{S}_2$. For reference, the Mn-S bond lengths in MnS_2 are given (solid line).

phur ions are bonded, via another sulphur ion, to a second transition metal ion. In the antiferromagnetic MnS_2 cell, the transition metal ions each have the same six distinct NN Mn-S bond lengths which vary between 2.56–2.60 Å. When the Mn^{2+} ions are substituted by Fe^{2+} in $\text{Fe}_x\text{Mn}_{1-x}\text{S}_2$ this degeneracy is broken and the lattice deforms differently around each transition metal ion.

In Fig. 6 the six NN TM-S bond lengths for each transition metal ion are presented, in increasing order, for the $\text{Mn}^{\text{HS}}\text{Fe}^{\text{HS}}$ state with compositions $x=0.25, 0.50,$ and 0.75 at $p=0$. As a reference, the bond lengths of Mn-S bond in pure MnS_2 are given by a solid line. Since the spin transition pressure for the Mn^{2+} ion decreases when Fe is introduced into the lattice, one might expect the Mn-S bonds to be shorter in $\text{Fe}_x\text{Mn}_{1-x}\text{S}_2$ than in pure MnS_2 . However, we see a more complicated development of the Mn-S bond lengths as the Mn^{2+} ions are substituted with Fe^{2+} . In the uppermost

curve, for $x=0.25$, two NN Mn-S bonds have increased compared to MnS_2 . These are the bonds which are connected to a sulphur-surrounded Fe^{2+} ion. As a Fe ion slightly contracts its octahedral sulphur environment, the neighboring Mn-S bond is extended. Nevertheless, for $x=0.25$, the majority of the Mn-S bonds decrease.

The same phenomena is observed for composition $x=0.50$, where three Mn-S bonds out of six are extended while the remaining three are contracted compared to MnS_2 . Thus, we are faced with the puzzling fact that for the four Mn^{2+} ions in the cell, their *average* Mn-S bond has not decreased. We therefore conclude that, in the case of $x=0.50$, the spin crossover is primarily driven by the electronic state of the Fe^{2+} ion. There are four Fe^{2+} ions/cell which experience extended Fe-S bonds ($\text{Fe-S} \approx 2.45\text{--}2.54$ Å) compared to their length in FeS_2 of 2.26 Å (cf. Table I). As pressure increases, the crystal field splitting in Fe^{2+} increases which causes the Fe^{2+} spin transition and a contraction of the lattice. This will, in turn, decrease the Mn-S bonds and favor a spin crossover for the Mn^{2+} ion.

For the $x=0.75$ composition, the pyrite lattice is dominated by Fe^{2+} ions. The remaining two Mn^{2+} ions/cell exhibit smaller Mn-S bonds compared to their equilibrium state bond lengths. It is therefore expected that we observe a decrease in spin transition pressure compared to the pure MnS_2 .

Figure 7 shows the spin transition volume changes as a function of composition in the $\text{Fe}_x\text{Mn}_{1-x}\text{S}_2$ system. In the GGA, the $\text{Mn}^{\text{HS}}\text{Fe}^{\text{HS}}$ state is never stable. The volume of the equilibrium state $\text{Mn}^{\text{HS}}\text{Fe}^{\text{LS}}$ decreases when the Fe content increases which results in a continuous decrease of $\Delta V_p(\text{Mn}^{\text{HS}}\text{Fe}^{\text{LS}}\text{--Mn}^{\text{LS}}\text{Fe}^{\text{LS}})$ with x . For $U_{\text{Fe}}=3$ eV, the combined volume change (v_1+v_2) from $\text{Mn}^{\text{HS}}\text{Fe}^{\text{HS}}\text{--Mn}^{\text{HS}}\text{Fe}^{\text{LS}}$ and $\text{Mn}^{\text{HS}}\text{Fe}^{\text{LS}}\text{--Mn}^{\text{LS}}\text{Fe}^{\text{LS}}$ is approximately constant around $9\text{--}10$ Å³/f.u.

It is interesting to consider the energy differences at the spin transition pressure. It is often assumed that the spin transition occurs when the crystal field splitting overwhelms the Hund coupling, and the energy can be reduced by changing from HS to LS. However, as can be seen in Table II and

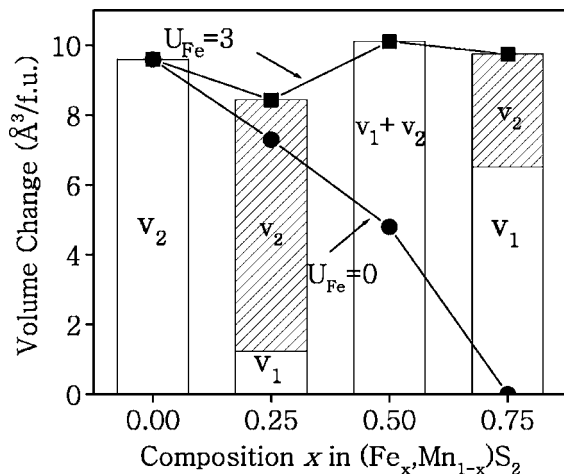


FIG. 7. Volume changes from $\text{Mn}^{\text{HS}}\text{Fe}^{\text{HS}}\text{--Mn}^{\text{HS}}\text{Fe}^{\text{LS}}$ (v_1) and $\text{Mn}^{\text{HS}}\text{Fe}^{\text{LS}}\text{--Mn}^{\text{LS}}\text{Fe}^{\text{LS}}$ (v_2) as a function of composition x in $\text{Fe}_x\text{Mn}_{1-x}\text{S}_2$ for $U_{\text{Fe}}=0$ and $U_{\text{Fe}}=3$ eV.

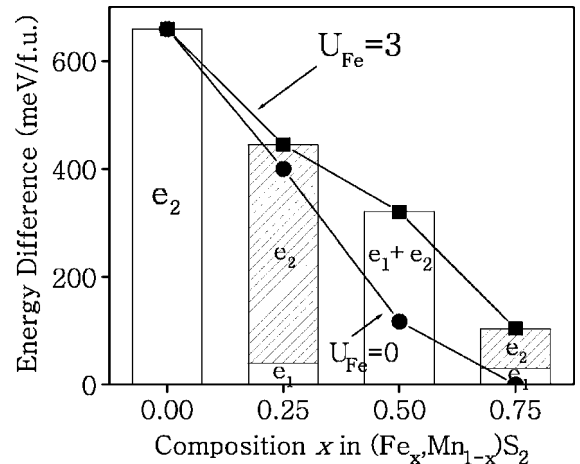


FIG. 8. Energy differences at the transition pressure between $\text{Mn}^{\text{HS}}\text{Fe}^{\text{HS}}$ and $\text{Mn}^{\text{HS}}\text{Fe}^{\text{LS}}$ (e_1) and $\text{Mn}^{\text{HS}}\text{Fe}^{\text{LS}}$ and $\text{Mn}^{\text{LS}}\text{Fe}^{\text{LS}}$ (e_2) as a function of composition x in $\text{Fe}_x\text{Mn}_{1-x}\text{S}_2$ for $U_{\text{Fe}}=0$ and $U_{\text{Fe}}=3$ eV.

Fig. 8, the energy difference between the HS and LS states is not zero at the transition pressure. The reason the transition occurs despite the increase in energy (or decrease, as in FeS_2), is that the enthalpy difference between HS and LS is zero at the transition pressure. In other words, it is the $p\Delta V_p$ HS-LS term in the enthalpy difference that balances the non-zero energy difference. If we consider the MnS_2 case, the energy difference between HS and LS at zero pressure is -720 meV/f.u. At the transition pressure this difference is still -660 meV/f.u., having changed by only 60 meV/f.u. The remaining -660 meV/f.u. is balanced by the $p\Delta V_p$ HS-LS term in the enthalpy difference. Therefore, it is clear that the $p\Delta V_p$ HS-LS term can play an essential role in driving the spin transition, and that simply considering the energy difference between the crystal field and Hund terms is likely to be inadequate. For MnS_2 , the $p\Delta V_p$ HS-LS term accounts for over 90% of the change in enthalpy required to drive the HS to LS transition.

IV. CONCLUSIONS

We have investigated spin transitions in mixtures of FeS_2 and MnS_2 . The system is designed to have two ionic species with very different equilibrium states. The Mn ion prefers the HS configuration which drives high unit cell volumes and the Fe ion prefers the LS configuration yielding low unit cell volumes. Thus, the spin transition scenario is highly dependent on the composition.

We find that the addition of a Hubbard U to the GGA formalism (with $U=3$ and $J=1$ eV) improves the agreement of the calculated ground state properties of FeS_2 with experiments, compared to GGA. Furthermore, when exploring Fe^{2+} substitution in MnS_2 , we observe that GGA+ U finds an equilibrium Fe^{2+} HS state in the expanded MnS_2 lattice as opposed to GGA.

The spin transition pressure decreases, in the $\text{Fe}_x\text{Mn}_{1-x}\text{S}_2$ system, with growing Fe content. For $U_{\text{Fe}}=0$, the $\text{Mn}^{\text{HS}}\text{Fe}^{\text{HS}}$ state is never realized for positive pressures and the spin cross-over occurs only for the Mn^{2+} ion. When the Fe d orbitals are described by a weak Hubbard U , the spin transition occurs in both transition metal ions, either separately at distinct pressures, or collectively at a common pressure. Independent of $0 \leq U_{\text{Fe}} \leq 3$ eV, there exists a composition for which a spin transition pressure approaches zero.

Monitoring the Mn-S bond lengths in HS $\text{Fe}_x\text{Mn}_{1-x}\text{S}_2$, as Fe^{2+} is introduced into the lattice, we find on average a weak decreasing trend with increasing Fe content. However, a more pronounced effect of the Fe substitution is the response of the Mn-S bonds to their different local environments. Thus, some Mn-S bonds actually increase around a Fe^{2+} ion, compared to the bond length in MnS_2 . The Fe-S bonds in the $\text{Mn}^{\text{HS}}\text{Fe}^{\text{HS}}$ state exhibit the expected overall increase compared to their $p=0$ bond length in FeS_2 . We conclude that the decrease of the spin transition pressure for the Mn^{2+} ion is not only caused by decreasing Mn-S bonds but also depend

on the pressure-induced spin transition of the Fe^{2+} ion. We find that at the spin transition pressure the energy of the HS and LS states are not at all equal and the $p\Delta V_p$ contribution to the enthalpy is the dominant driving force for the transition. Hence, simple physical arguments based on crystal field splitting and Hund's coupling cannot accurately describe the transition pressure.

The development of the spin transition volume change as a function of composition is found to be highly dependent on whether the Fe d orbitals are described with the GGA and GGA+ U formalism. For $U_{\text{Fe}}=0$, the Fe^{2+} ions are LS, and the only volume effect is due to the spin cross-over in the Mn^{2+} ion. Thus, as the Mn content decreases, so does the volume change at the transition. When $U_{\text{Fe}}=3$ eV is applied, the combined volume change for the HS-LS transition is approximately constant and around $9-10 \text{ \AA}^3/\text{f.u.}$ This is a particularly large volume change and may be of practical use in applications.

In conclusion, we have demonstrated an approach to tuning spin transition pressures through alloying. Our results point to a way of designing materials where alloying may bring spin transitions into desired temperature and pressure ranges.

ACKNOWLEDGMENTS

Support from MIT Institute for Soldier Nanotechnologies, Grant No. DAAD19-02-D-0002 is gratefully acknowledged. Additional computing resources were provided by the National Science Foundation, National Partnership for Advanced Computing Infrastructure (NPACI).

APPENDIX: ORDERED ARRANGEMENTS IN $\text{Fe}_x\text{Mn}_{1-x}\text{S}_2$

The lattice vectors of the tetragonal 24 atom unit cell of $\text{Fe}_x\text{Mn}_{1-x}\text{S}_2$ are $\mathbf{a}=(2,0,0)a$, $\mathbf{b}=(0,1,0)a$, and $\mathbf{c}=(0,0,1)a$. In this lattice, the ideal (unrelaxed) atomic positions of the eight transition metal ions in Cartesian coordinates are

$$A^{(1)} = (0,0,0)a, \quad A^{(2)} = (1.0,0,0)a,$$

$$A^{(3)} = (0,0.5,0.5)a, \quad A^{(4)} = (1.0,0.5,0.5)a,$$

$$A^{(5)} = (0.5,0,0.5)a, \quad A^{(6)} = (1.5,0,0.5)a,$$

$$A^{(7)} = (0.5,0.5,0)a, \quad A^{(8)} = (1.5,0.5,0)a.$$

For the $x=0.25$ ($x=0.75$) composition in the first arrangement the $A^{(1)}-A^{(2)}$ positions are occupied by Fe(Mn) atoms. In the second arrangement the $A^{(1)}$ and $A^{(5)}$ positions are selected for the minority species.

For the $x=0.50$ composition the first arrangement puts the Fe atoms at $A^{(1)}-A^{(4)}$, while in the second arrangement the $A^{(1)}$, $A^{(3)}$, $A^{(4)}$, and $A^{(5)}$ positions are decorated with Fe atoms.

- ¹R. E. Cohen, I. Mazin, and D. G. Isaak, *Science* **275**, 654 (1997).
- ²M. P. Pasternak, R. D. Taylor, R. Jeanloz, X. Li, J. H. Nguyen, and C. A. McCammon, *Phys. Rev. Lett.* **79**, 5046 (1997).
- ³J. Badro, G. Fiquet, F. Guyot, J.-P. Rueff, V. V. Struzhkin, G. Vankó, and G. Monaco, *Science* **300**, 789 (2003).
- ⁴C. Zobel, M. Kriener, D. Bruns, J. Baier, M. Grüniger, and T. Lorenz, *Phys. Rev. B* **66**, 020402(R) (2002).
- ⁵J.-Q. Yan, J.-S. Zhou, and J. B. Goodenough, *Phys. Rev. B* **69**, 134409 (2004).
- ⁶P. G. Radaelli and S.-W. Cheong, *Phys. Rev. B* **66**, 094408 (2002).
- ⁷I. Troyan, A. G. Gavrilyuk, V. A. Sarkisyan, I. S. Lyubutin, R. Ruffer, O. Leopold, A. Barla, B. Doyle, and A. I. Chumakov, *JETP Lett.* **74**, 26 (2001).
- ⁸W. M. Xu, O. Naaman, G. K. Rozenberg, M. P. Pasternak, and R. D. Taylor, *Phys. Rev. B* **64**, 094411 (2001).
- ⁹A. G. Gavriliuk, I. A. Troyan, R. Boehler, M. I. Eremets, I. S. Lyubutin, and N. R. Serebryanaya, *JETP Lett.* **77**, 747 (2003).
- ¹⁰P. Ravindran, H. Fjellvåg, A. Kjekshus, P. Blaha, K. Schwarz, and J. Luitz, *J. Appl. Phys.* **91**, 291 (2002).
- ¹¹J. G. Drickamer and C. W. Frank, *Electronic Transitions and the High Pressure Chemistry and Physics of Solids* (Chapman and Hall, London, 1973).
- ¹²O. Kahn and C. J. Martinez, *Science* **279**, 44 (1998).
- ¹³J. M. Hastings, N. Elliott, and L. Corliss, *Phys. Rev.* **115**, 13 (1959).
- ¹⁴J. M. Hastings and L. M. Corliss, *Phys. Rev. B* **14**, 1995 (1976).
- ¹⁵T. Chattopadhyay, H. von Schnering, and H. A. Graf, *Solid State Commun.* **50**, 865 (1984).
- ¹⁶J. E. F. Westrum and F. Grenvold, *J. Chem. Phys.* **52**, 3870 (1970).
- ¹⁷J. Rossat-Mignod, *Neutron Scattering* (Academic, Orlando, 1986).
- ¹⁸T. Chattopadhyay, T. Brüchel, and P. Burellet, *Phys. Rev. B* **44**, 7394 (1991).
- ¹⁹T. Chattopadhyay and H. G. von Schnering, *J. Phys. Chem. Solids* **46**, 113 (1985).
- ²⁰T. Chattopadhyay, H. G. von Schnering, and W. A. Grosshans, *Physica B & C* **139-140**, 305 (1986).
- ²¹A. Rohrbach, J. Hafner, and G. Kresse, *J. Phys.: Condens. Matter* **15**, 979 (2003).
- ²²P. Vulliet, J. P. Sanchez, D. Braithwaite, M. Amanowics, and B. Malaman, *Phys. Rev. B* **63**, 184403 (2001).
- ²³H. Fjellvåg, A. Kjekshus, T. Chattopadhyay, H. D. Hochheimer, W. Hönle, and H. G. von Schnering, *Physica B & C* **139-140**, 305 (1986).
- ²⁴T. Chattopadhyay, H. G. von Schnering, R. F. D. Stansfield, and G. J. McIntyre, *Z. Kristallogr.* **199**, 13 (1992).
- ²⁵E. D. Stevens, M. L. DeLucia, and P. Coppens, *Inorg. Chem.* **19**, 813 (1980).
- ²⁶S. Merkel, A. P. Jephcoat, J. Shu, H.-K. Mao, P. Gillet, and R. J. Hemley, *Phys. Chem. Miner.* **29**, 1 (2002).
- ²⁷M. S. Lin and H. J. Hacker, *Solid State Commun.* **6**, 687 (1968).
- ²⁸G. Brostigen and A. Kjekshus, *Acta Chem. Scand.* (1947-1973) **5**, 2993 (1970).
- ²⁹R. K. Li, K. Johnson, D. E. Eastman, and J. L. Freeouf, *Phys. Rev. Lett.* **32**, 470 (1974).
- ³⁰S. L. Finklea, L. Cathey, and E. L. Amma, *Acta Crystallogr., Sect. A: Cryst. Phys., Diffraction, Theor. Gen. Crystallogr.* **A32**, 529 (1976).
- ³¹C. B. Barger, M. Avinor, and H. G. Drickamer, *Inorg. Chem.* **10**, 1338 (1971).
- ³²M. A. S. Kahn, V. H. McCann, J. B. Ward, and R. J. Pollard, *J. Phys. C* **16**, 4011 (1983).
- ³³P. E. Blöchl, *Phys. Rev. B* **50**, 17953 (1994).
- ³⁴G. Kresse and D. Joubert, *Phys. Rev. B* **59**, 1758 (1999).
- ³⁵G. Kresse and J. Furthmüller, *Phys. Rev. B* **54**, 11169 (1996).
- ³⁶G. Kresse and J. Furthmüller, *Comput. Mater. Sci.* **6**, 15 (1996).
- ³⁷H. J. Monkhorst and J. D. Pack, *Phys. Rev. B* **13**, 5188 (1976).
- ³⁸P. E. Blöchl, O. Jepsen, and O. K. Andersen, *Phys. Rev. B* **49**, 16223 (1994).
- ³⁹J. P. Perdew, K. Burke, and M. Ernzerhof, *Phys. Rev. Lett.* **77**, 3865 (1996).
- ⁴⁰A. I. Liechtenstein, V. I. Anisimov, and J. Zaanen, *Phys. Rev. B* **52**, R5467 (1995).
- ⁴¹D. Morgan, S. Curtarolo, and G. Ceder (2005), <http://burgaz.mit.edu/CODES/>
- ⁴²D. Hobbs and J. Hafner, *J. Phys.: Condens. Matter* **11**, 8197 (1999).
- ⁴³F. D. Murnaghan, *Proceedings of the National Academy of Sciences* (1944), Vol. 30, p. 244.
- ⁴⁴Y. Zeng and N. A. W. Holzwarth, *Phys. Rev. B* **50**, 8214 (1994).
- ⁴⁵V. Eyert, K.-H. Höck, S. Fiechter, and H. Tributsch, *Phys. Rev. B* **57**, 6350 (1998).
- ⁴⁶H. M. Sithole, D. Nguyen-Manh, D. G. Pettifor, and P. E. Ngoepe, *Mol. Simul.* **22**, 31 (1999).
- ⁴⁷I. Opahle, K. Koepnik, and H. Eschrig, *Phys. Rev. B* **60**, 14035 (1999).
- ⁴⁸J. Muscat, A. Hung, S. Russo, and I. Yarovsky, *Phys. Rev. B* **65**, 054107 (2002).
- ⁴⁹H. M. Sithole, P. E. Ngoepe, and K. Wright, *Phys. Chem. Miner.* **30**, 615 (2003).